Discover Chemical Engineering

Discover

Perspective

Rational design of iron single-atom catalysts for electrochemical nitrate reduction to produce ammonia

Xi Chen[1] · Xinlei Ji[1] · Jia Kou[1]

Received: 30 October 2023 / Accepted: 13 December 2023
Published online: 15 December 2023

Abstract
Ammonia (NH_3) is the second-most produced chemical with broad applications and vital for the chemical industry. However, the current Haber–Bosch synthesis is problematic with high energy consumption and carbon footprints. Electrochemical nitrate reduction (NO_3RR) to produce NH_3 is a green, low-carbon and efficient alternative route to simultaneously benefit wastewater treatment, mild NH_3 production and global warming mitigation. Compared to noble metal catalysts or the nanosized counterparts, iron single-atom catalysts (Fe SACs) boast unique advantages to promote the NO_3RR because of the exceptional selectivity, inexpensiveness, high efficiency and good durability. Due to the rapid development of the emerging field, a timely Perspective with an emphasis on the recent advances in Fe SACs-catalyzed NO_3RR is currently lacking. The Perspective aims to give an account of the up-to-date progresses on Fe SACs-promoted NO_3RR for NH_3 production. The catalyst design, characterizations, mechanism studies, etc. will be illustrated, and lastly the challenges and outlook will be discussed to provide insights for future studies.

1 Introduction

Ammonia (NH_3) is one of the most prime substances in the chemical industry. With broad applications in various end-use areas such as fertilizers, pharmaceuticals and precursors for fine organonitrogen chemicals, the global market size of NH_3 is estimated to be ~ US$ 76 billion in 2022 and expected to reach US$ 104 billion in the next 5 years. Moreover, NH_3 has been regarded as a promising carbon-free energy carrier for hydrogen because of its high hydrogen content (~ 18 wt%), good stability for transportation, well-established infrastructures, etc. which could play a critical role in the energy transit for shaping a sustainable future [1–3]. However, the current NH_3 production and utilization mode suffer from some major obstacles which has induced vital environmental issues. The large-scale NH_3 production in industry primarily relied on the Haber–Bosch process in the past century. The Haber–Bosch process is usually catalyzed by an iron (Fe)-based catalyst under rather harsh conditions (such as 400–500 °C, 15–30 MPa), which is energy-intensive with high carbon footprints. As estimated, the NH_3 synthesis process accounts for 1–2% of the world's total energy consumption as well as ~ 1% of the global carbon dioxide (CO_2) emission. Hence, the current synthesis protocol is against the green chemistry principle and notably deteriorates the global warming and climate change. At downstream end, the anthropogenic activities of using NH_3 as fertilizers and other chemicals have seriously disturbed the natural nitrogen cycle, releasing considerable amounts of nitrate into the environment. The nitrate is relatively stable and could accumulated in water systems to cause eutrophication and damage the aquatic ecosystems, in addition, to pose threats to the health human beings through drinking. Besides, the more toxic water pollutant nitrite could be generated from nitrate which

✉ Xi Chen, chenxi-lcc@sjtu.edu.cn; Xinlei Ji, xinlei.ji@sjtu.edu.cn; Jia Kou, koujia2022@sjtu.edu.cn | [1]China-UK Low Carbon College, Shanghai Jiao Tong University, 3 Yinlian Rd, Shanghai 201306, China.

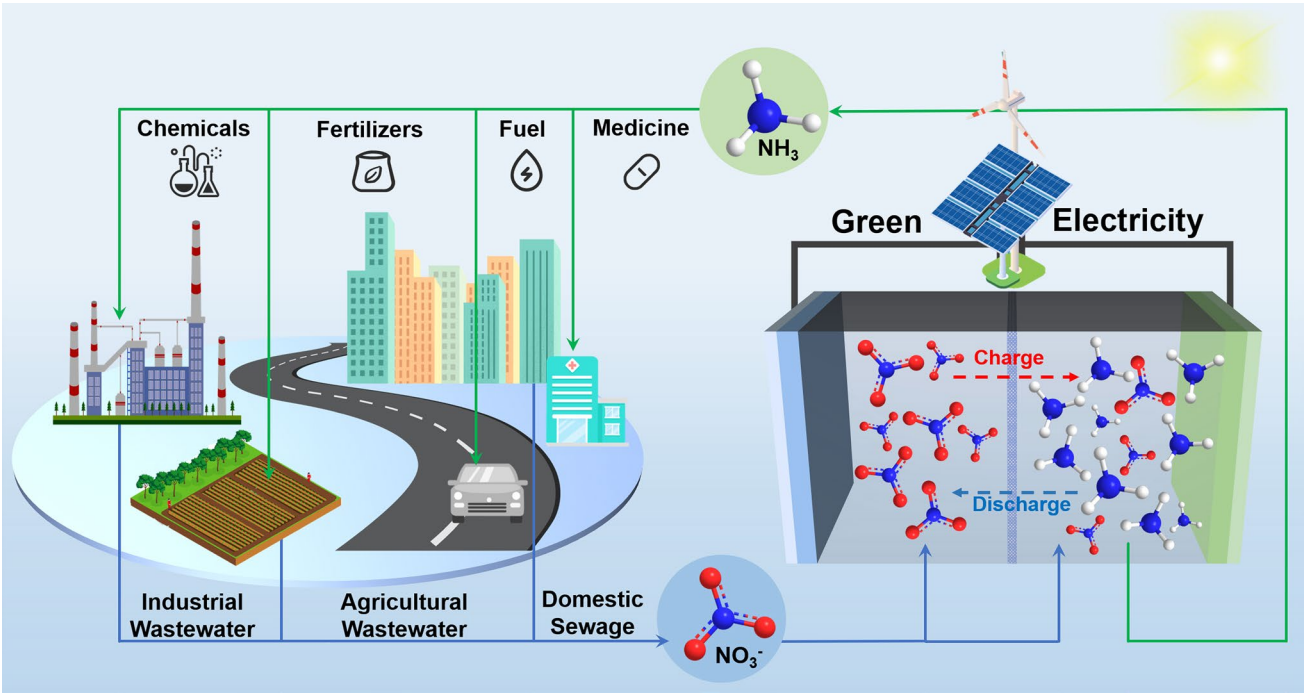

Scheme 1 The overview of NO_3RR for simultaneous wastewater treatment and global warming mitigation to produce NH_3. The municipal wastewater will be employed as the feedstock and undergo NO_3RR with green electricity for NH_3 production to achieve the closed nitrogen cycle

is a carcinogenic compound. As a result, nitrate removal in water treatment is of great importance to restore the balance of nitrogen cycle and protect the water systems.

Renewable approaches to produce organonitrogen compounds from biomass have been devised [4–20], while the NO_3RR which employs green electricity to upgrade nitrate as the water pollutants into NH_3 under mild conditions (normally ambient pressure and room temperature) without forming other harmful by-products is regarded as the most prominent alternative method to Haber–Bosch process and has drawn significant attentions [21–27]. Traditional nitrate removal adopts the denitrification pathway to generate non-harmful nitrogen gas (N_2) for environmental remediation [28]. In addition, the electrochemical nitrogen reduction (NRR) has been extensively explored as an alternative route for NH_3 production but the conversion is relatively challenging and the production rate is usually low due to the inactiveness of nitrogen gas (the triple bond energy of ~ 941 kJ/mol). The NO_3RR furnishes an exceptional solution to shoot two hawks with one arrow, which could simultaneously achieve nitrate removal for wastewater treatment and low-carbon NH_3 production in a more desirable manner (see Scheme 1). Converting nitrate to NH_3 rather than N_2 is less difficult and could upcycle the waste pollutant into a valuable chemical commodity. Nitrate is highly soluble in aqueous solutions and possesses much lower bond energies (~ 204 kJ/mol for N=O bond and ~ 176 kJ/mol for N–O bond), and thus serves as a more suitable and advantageous feedstock for practical large-scale NH_3 production. As a result, the NO_3RR technology represents a green, mild and economic way to refresh the current NH_3 industry remarkably contributing to global warming mitigation and restore the nitrogen cycle for environmental protection.

Catalyst design and development is key to achieve efficient and selective NO_3RR for NH_3 production. So far, metal-free carbon-based catalysts, the diverse noble and non-noble metal species (Pd, Pt, Ru, Ti, Ni, Fe, Cu, etc.) as nanoparticles (NPs) or SACs and their bimetallic or trimetallic counterparts have been reported to promote the reaction. The non-noble iron-based catalysts have been long-standing employed for industrial catalytic processes including the Haber–Bosch reaction, which boast principal merits among the reported metal species for NO_3RR due to the abundance (the second most abundant metal element in the Earth's crust), broad availability, low price, nontoxicity and high catalytic performance. Nonetheless, the Fe NPs catalysts suffer from major problems including the surface oxidation (deactivation) and the lack of selectivity towards NH_3 (N_2 is often a noticeable side product). Fe SACs possess outstanding merits to overcome these obstacles. The concept of SACs was officially coined by Zhang's group in 2011 [29–31], which denotes as atomically-dispersed metal atoms on a support with 100% exposure of the active sites (100% atom efficiency) [32]. Lacking the neighboring Fe atoms would suppress the N–N coupling reaction and prevent the formation of N_2 by-product.

Hence, Fe SACs could lead to a very high NH_3 selectivity. The Fe SACs are often stabilized by the strong metal-support interactions (SMSI) by coordinating with heteroatoms such as N, O, etc. The Fe SACs originally possess high valence state and thus oxidation is not a concern herein. The high valence and exclusive quantum confinement effect have maximized the surface free energy of the Fe sites endowing them with a high catalytic activity.

With these salient features, Fe SACs have emerged as new catalyst materials for efficient NO_3RR in the past 3 years. Most of the Fe sites were anchored on carbon-based support due to their high conductivity, tunable surface groups, porosity, cheap price and stability. The rational design of the Fe SACs is fundamental to achieve the high NH_3 production rate, high FE, outstanding stability and low overpotential. The coordination environment of Fe SACs with special electronic and chemical states will significantly affect the reaction barriers, kinetics and pathways. The finely-tuning of the coordination atoms (the number and species) is one of the key strategies for the development of Fe SACs for NO_3RR. Besides, the Fe loading is also a primary factor that high loading of Fe SACs usually leads to better electrochemical performance due to the presence of ample active sites. In addition, the properties of the support such as the pore structure, graphitization degree, surface functional groups, electron transfer ability, etc. are highly related to the catalytic activity. Various synthetic procedures have been devised to design Fe single atom sites with different coordination patterns and to result in carbon-based supports with distinct characters. So far, there are many excellent reviews on electrocatalytic NO_3RR but a timely Perspective with an emphasis on the Fe SACs has not yet been reported. This perspective gives a brief account on the recent advances in Fe SACs-catalyzed NO_3RR, which is mainly progressed in the past 3 years. The preparation methods, catalyst design tactics, characterization tools, electrochemical performances as well as the reaction mechanisms will be illustrated. The challenges, future directions for rational catalyst design and opportunities are outlooked, with the expectation to provide a timely summary to shed some light on the emerging and propitious field of Fe SACs-catalyzed NO_3RR.

2 The mechanistic aspects

The NO_3RR to convert nitrate into NH_3 requires the transfer of nine protons along with eight electrons. The equations of the overall reaction (Equation 1) and the elementary steps (Equations 2–9) were shown in Fig. 1. The active adsorbed hydrogen is regarded as a key intermediate for NO_3RR, which is derived from water upon adsorption and reduction on the electrode surface. The nitrate and adsorbed hydrogen species would react and steadily produce NH_4^+ through multiple intermediates such as NO_2^*, NO^*, N^*, NH^*, NH_2^*, etc. Note that NH_3 and N_2 are both the most thermodynamically stable forms of the reduced products, and the avoidance of N_2 formation is necessary to maintain a high selectivity

Fig. 1 The equations of the overall reaction and the elementary steps for NO_3RR (Reprinted with permission from Ref. [21]. Copyright 2023 the Royal Society of Chemistry)

$$NO_3^- + 9H^+ + 8e^- \rightarrow NH_3 + 3H_2O \quad (1)$$

$$NO_3^- + 2H^+ + 2e^- \rightarrow NO_2^- + H_2O \quad (2)$$

$$NO_3^-{}_{ad.} + e^- \rightarrow NO_3^{2-}{}_{ad.} \quad (3)$$

$$NO_3^{2-}{}_{ad.} + 2H^+ \rightarrow NO_2\bullet + H_2O \quad (4)$$

$$NO_2\bullet{}_{ad.} + e^- \rightarrow NO_2^-{}_{ad.} \quad (5)$$

$$NO_{ad.} + H^+ + e^- \rightarrow HNO_{ad.} \quad (6)$$

$$HNO_{ad.} + H^+ + e^- \rightarrow H_2NO_{ad.} \quad (7)$$

$$H_2NO_{ad.} + H^+ + e^- \rightarrow NH_2OH_{ad.} \quad (8)$$

$$NH_2OH_{ad.} + 2H^+ + 2e^- \rightarrow NH_3 + H_2O \quad (9)$$

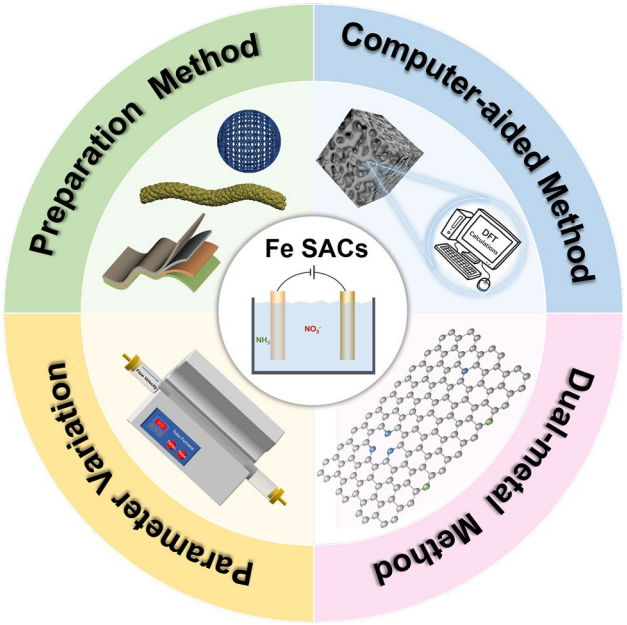

Scheme 2 The different strategies for the design of Fe SACs (including the preparation method, parameter variation, dual-metal method and computer-aided method)

to NH_3 in NO_3RR. Except for N_2, other minor side products such as nitrite and hydrazine could also be produced during the NO_3RR to lower down the NH_3 selectivity. Another side reaction that often affects the product selectivity is the HER which happened at high overpotential to consume the active hydrogen species and compete with the NH_3 formation, resulting in declined Faradaic efficiency (FE). Overall, the NO_3RR involves complexes processes with multiple transportation of protons and electrons, and thus the acceleration of the reaction kinetics and the suppression of side reactions are the pivotal tasks for enhanced NO_3RR performance. The NO_3RR efficiency and selectivity is highly relied on the catalyst materials, and the rational designs and developments of heterogeneous catalysts for NO_3RR is paramount to boost the reaction rate, mitigate the overpotential, increase the FE and NH_3 selectivity.

3 Catalyst design of Fe SACs for NO_3RR

To improve the catalytic performance of Fe SACs, the preparation of carbon support, the parameter variation, the design of dual-metal catalysts and the computer-aided method have been so far employed for the rational design of Fe SACs (see Scheme 2). Table 1 has summarized the recent works of Fe SACs-catalyzed NO_3RR to compare the catalyst species, performance and stability.

Characterizations of the Fe SACs are very important, especially the unique techniques to reveal the single atom nature of the as-synthesized catalysts. Generally, the transmission electron microscopy (TEM), X-ray diffraction (XRD) and X-ray photoelectron spectroscopy (XPS) are first employed to demonstrate the high dispersion of the catalysts. Normally, the clusters or NPs will be absent on TEM images and the corresponding signals will be negligible on XRD to indicate the single atom nature. The high valence of Fe signal should be observed on XPS since the Fe SACs is usually positively charged. Next, advanced techniques such as the aberration-corrected high-angle-annular-dark-field scanning transmission electron microscopy (AC-HAADF-STEM) is adopted to directly display the images of SACs at an atomic level. Besides, the X-ray absorption spectroscopy (XAS) is adopted to gain further information on the coordination environment of Fe SACs. The X-ray absorption near edge spectroscopy (XANES) discloses the valence states, geometry information, etc., and the extended X-ray absorption fine structure (EXAFS) reveals the coordination atoms and numbers, etc. These are the most common characterization methods for SACs analysis.

Pioneering studies of Fe SACs-catalyzed NO_3RR have been reported in 2021. Siahrostami and Wang's group have synthesized carbon-supported Fe SACs by pyrolysis which exhibited high selectivity and activity to convert nitrate into NH_3 under ambient environment [33]. The maximal FE was ~ 75% at − 0.66 V with the highest NH_3 production rate of ~ 20 $mg/h/mg_{cat}$. (0.46 $mmol/h/cm^2$) at − 0.85 V. The Fe SACs maintained stable performances after 20 cycle numbers. The Fe SACs were prepared by a transition metal-assisted carbonization method with mixed precursors of $FeCl_3$ and *o*-phenylenediamine and SiO_2 powders as the hard templates. Following the pyrolysis, etching with both strong base

Table 1 Recent works of Fe SACs-catalyzed NO_3RR

Entry	Catalyst species	Reaction conditions	NH_3 FE	NH_3 yield rate (mg/h/$g_{cata.}$)	NH_3 selectivity	Durability	Ref.
1	Fe-OPD SAC	0.5 M KNO_3/0.1 M K_2SO_4 0.5 h	~75.00% at − 0.66 V vs. RHE	~20 at − 0.85 V vs. RHE	~75.00% at − 0.66 V vs. RHE	20 cycles	[33]
2	Fe-PPy SAC	0.1 M KOH + 0.1 M KNO_3 0.5 h	99.69% at − 0.3 V vs. RHE	~12.26 at − 0.7 V vs. RHE	Over 80% at all potentials	9 cycles	[34]
3	Fe-CNS SAC	~0.007 M N-NO_3^- + 0.02 M Na_2SO_4/ NaCl	~78.4% at − 0.57 V vs. RHE	–	100% lower than − 0.57 V vs. RHE	5 cycles	[35]
4	Fe-N/P-C SAC	0.1 M KOH + 0.1 M KNO_3 0.5 h	90.3% at − 0.4 V vs. RHE	~18.0 at − 0.8 V vs. RHE	90% at − 0.4 V vs. RHE	20 cycles	[36]
5	Fe-N_2O_2-C SAC	0.5 M KNO_3 + 0.1 M K_2SO_4 0.5 h	92% at − 0.68 V vs. RHE	~46 at − 0.88 V vs. RHE	~96% at − 0.68 V vs. RHE	15 cycles	[37]
6	Fe-NC-900 SAC	0.1 M K_2SO_4 + 0.5 M KNO_3 1 h	~86% at − 0.7 V vs. RHE	~18.8 at − 0.9 V vs. RHE	–	20 cycles	[38]
7	Fe-algae SAC	~0.02 M NO_3^- + 1 M KOH 4 h	87.3% at − 0.42 V vs. RHE	20.44 at − 0.42 V vs. RHE	88% at − 0.42 V vs. RHE	Continuous operation over 50 h	[39]
8	Fe-g-C_3N_4 SAC	~0.004 M N-NO_3^- + 0.1 M Na_2SO_4 24 h	77.3% at − 0.65 V vs. RHE	–	98.6% at − 0.65 V vs. RHE	8 cycles	[40]
9	Fe-MXene SAC	~0.004 M N-NO_3^- + 0.1 M Na_2SO_4 10 h	− 82.9% at − 1.2 V vs. Ag/AgCl	–	99.2% at − 1.4 V vs. Ag/AgCl	Continuous electrolysis for 10 h	[41]
10	$FeCl_2$-PTI SAC	0.1 M PB + 0.1 M KNO_3	80% at 0.80 V vs. RHE	4.26 at 0.80 V vs. RHE	–	–	[42]
11	Fe/Cu-HNG SAC	1 M KOH + 0.1 M KNO_3	92.51% at − 0.3 V vs. RHE	~63.4 at − 0.5 V vs. RHE	–	Continuous electrolysis for 24 h	[43]

and acid to remove any formed NPs and the SiO_2 templates, and a second pyrolysis treatment to lessen the inactive Fe sites after etching have been conducted (see Fig. 2a). Obvious NPs were negligible in the TEM image (see Fig. 2b), and the AC-MAADF-STEM together with EDS and EELS (see Fig. 2c–e) suggested the atomically dispersed Fe atoms on the interconnected, porous vesicle-like carbon support. The BET surface area was determined to be ~ 286 m^2/g with the mesopore size distribution centered at 18.3 nm. The Fe loading was about 1.5 wt% by ICP-OES analysis. The EELS on the single Fe site suggests the Fe-N-C coordination structure, which was further verified by XPS and XAS. The Fe single atoms were in high valence states and Fe–Fe bond was negligible. Fe-N_4 coordination environment was suggested by the fitting analyses. The Co and Ni SACs were synthesized for comparison and Fe SACs displayed much superior NH_3 yield rate (almost four-time to those using Co and Ni SACs). The DFT calculations implies that the Fe SAC site was intrinsically more active than the Fe NPs, Co and Ni SAC site with lower thermodynamic barriers. The possible rate-determining steps of NO_3RR on Fe SACs were calculated to be the reduction reactions of the NO^* and HNO^* species, which were different from those on Fe NPs. The study has pointed out the great potential of carbon-supported Fe SACs in NO_3RR.

Li et al. devised a polymer-hydrogel strategy to prepare *N*-coordinated Fe SACs on carbon support using the ferric acetylacetone and polypyrrole hydrogel precursors through adsorption and calcination [34]. About 100% FE after − 0.3 V and ~ 510 mg/h/mg_{Fe} (0.16 mmol/h/cm^2) NH_3 production rate at − 0.7 V were achieved under alkaline conditions. The durability tests revealed only a minor fluctuation within 10 cycles. The sheet-like porous morphology of the carbon support was observed on SEM images, and the HAADF-STEM images suggested the single-atom nature of the Fe sites with a

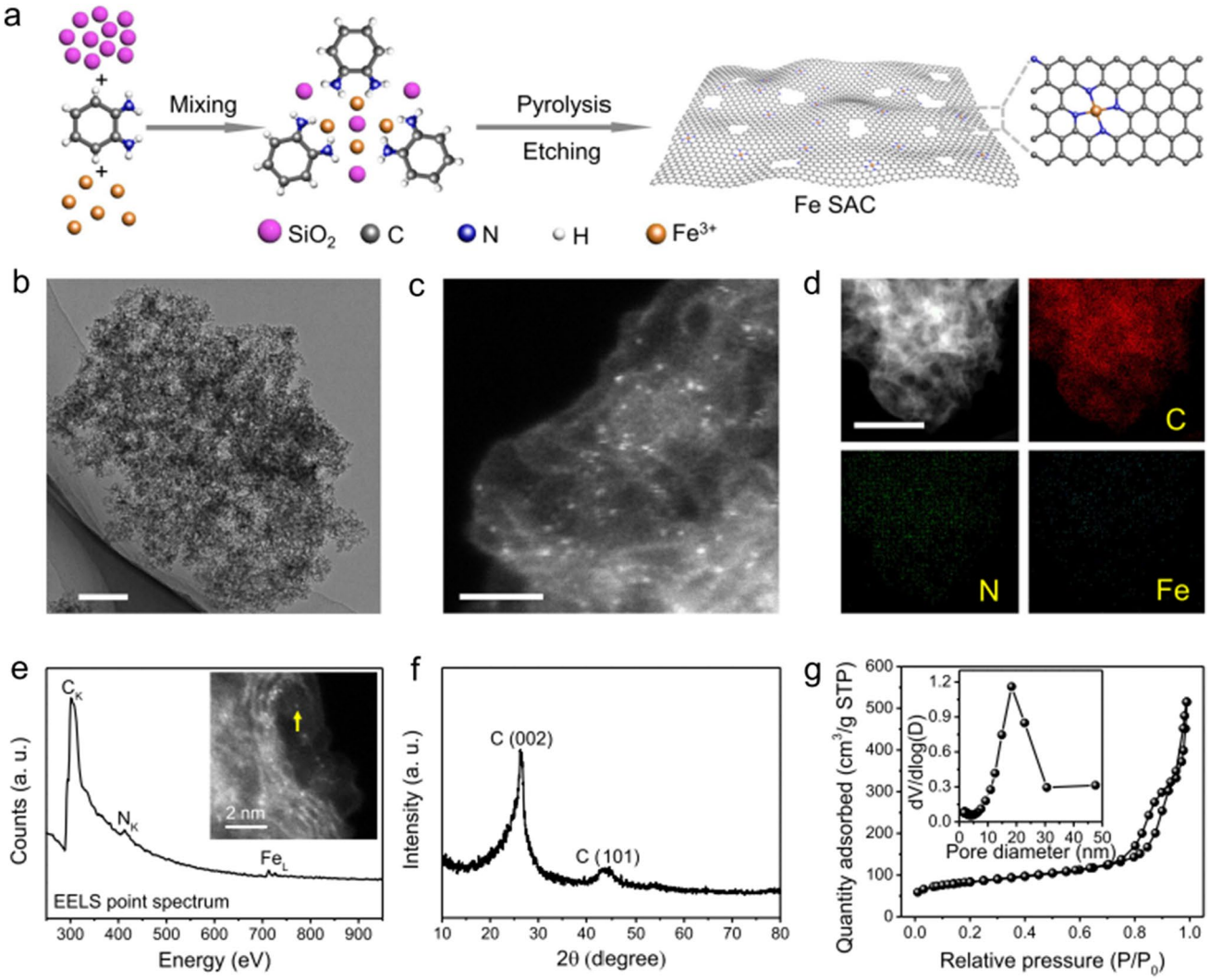

Fig. 2 **a** Schematic illustration for Fe SACs synthesis; **b** TEM image; **c** AC-MAADF-STEM image; **d** EDS mapping image; **e** EELS point spectrum; **f** XRD pattern; **g** N_2 adsorption–desorption isotherms (Reprinted with permission from Ref. [33]. Copyright 2021 the Springer Nature)

good loading of about 2.4 wt% (by ICP-MS). XPS analysis shows the Fe^{2+} oxidation states which was confirmed by XAS, and Fe-N_4 coordination structure was deduced based on the fitting results. The SI-SECM, which serves as an in-situ technique to accurately measure the amount of charge passed to a starting catalyst layer and give insights into the kinetic behaviors, has been adopted to study the reaction mechanisms. The reaction rates of nitrate binding to Fe(II)-Nx and Fe(0)-Nx model were 0.057 and 1.24 s^{-1}, whereas such catalytic activity was not observed for Fe NPs regardless of the delay time. Besides, the Fe-N sites would not induce the water dissociation as the side reaction. The experimental results also pointed out a nearly 12-time higher reaction rate of Fe single atoms compared to that of the bulk Fe surface. According to the DFT calculations, the single Fe atom adsorbed the NO_3^- in the way of the end-on mode whereas the Fe NPs bonded to two O atoms due to the existing adjacent Fe atoms (see Fig. 3a, b). The partial density of states (PDOS) of Fe-PPy SACs and Fe NPs suggested that the NO_3^- activation was more beneficial on the Fe-PPy SACs (see Fig. 3c). The Gibbs free energy (see Fig. 3d) of NO_3^- adsorption on Fe PPy SACs was more negative than the value of water adsorption which indicates that the NO3RR is more favorable than the HER side reaction. The study put forward a novel polymer-hydrogel strategy to synthesize Fe SACs for NO_3RR which demonstrates the significance of preparation method to improve the reaction.

The influence of Fe coordination environment has been investigated by several studies. Li's group has adjusted the coordination environment of Fe sites and prepared N-doped and S,N-codoped carbon materials (Fe-CN and Fe-CNS) [35]. The NH_4Cl and urea were used as the N precursors and thiourea was supplemented as the S precursor for the codoped materials through the pyrolysis of pyromellitic dianhydride. The highest FE for NH_3 was obtained of ~ 78.4% at a low potential of − 0.57 V, and the maximal nitrate removal ability was 7822 mg N/g_{Fe}. Based on the TEM, HAADF-TEM and EELS

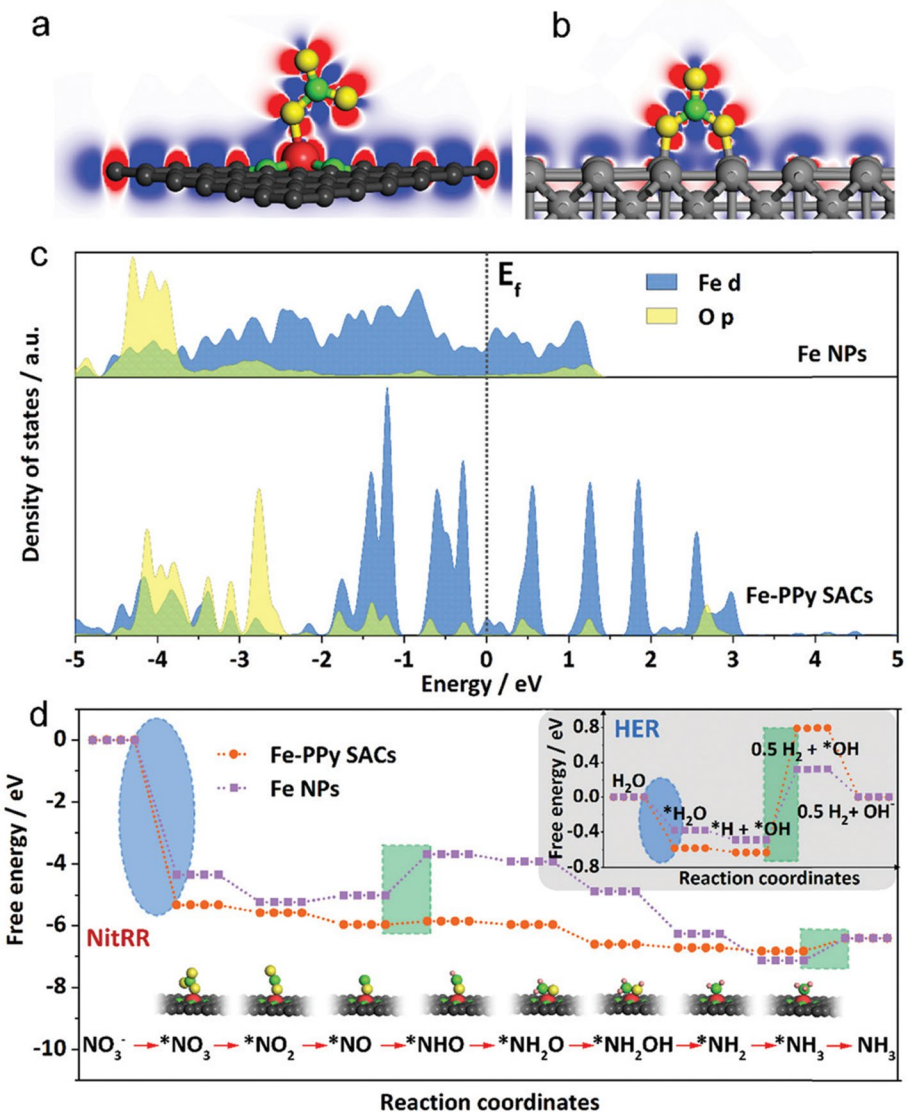

Fig. 3 The optimized charge density difference of **a** the Fe-PPy SACs and **b** Fe NPs; **c** PDOS of Fe d and O p of NO_3^--bonded to the Fe-PPy SACs and Fe NPs; **d** Gibbs free energy diagram of NO3RR to NH3 and water dissociation (the top right) (Reprinted with permission from Ref. [34]. Copyright 2021 the Royal Society of Chemistry)

analyses, the single atom states of Fe was substantiated, and Fe-N coordination was inferred for both Fe-CN and Fe-CNS. The Fe loading was about 2.1 wt% and 2.0 wt% for Fe-CN and Fe-CNS SACs by ICP-OES. As shown in Fig. 4, the XANES spectra of Fe-CN and Fe-CNS both displayed relatively high valence rather than the metallic state. Only Fe-N bonds were identified in the k^2-weighted EXAFS spectra without the formation of Fe–Fe bond or Fe-S bond. It is deduced that the S atom was bonded to the N atoms nearby the Fe single atoms (see Fig. 4e). The ^{57}Fe Mössbauer spectroscopy also indicates the absence of Fe–Fe bonds which was in agreement with the XAS data. The S co-doping brought about increased surface detects and affected the length of Fe-N bond, which induced asymmetric charge distribution and thus more prone to anchor metal atoms and modulate the surrounding environment. The Fe-CNS displayed superior catalytic activity to the Fe-CN, and uniquely tuned the product selectivity to NH_3 or N_2 at different potentials. The DFT simulation results show that the energy barriers for N^* to N_2^* and to NH^* on Fe-CNS were about − 0.14 and 2.78 eV and therefor the NH_3 path is more thermodynamically favorable. Xu et al. introduced P as a second coordinating heteroatom to Fe SAC and fabricated Fe-N/P-C structure [36]. The P atoms have interrupted the symmetric local charge of Fe SACs and promoted the surface adsorption of nitrate and other key intermediates to boost the NO_3RR efficiency. The Fe-N/P-C catalyst could achieve a high FE of 90.3% at − 0.4 V with NH_3 production rate of 18.0 mg/h/mg_{cat} at − 0.8 V. The *operando* SR-FTIR analyses and DFT calculations have been utilized to reveal the reaction pathway and the crucial role of the asymmetric configuration has been proved. These works have contributed to the fundamental understanding of heteroatom doping (such as S, P, etc.) in the carbon materials for Fe SACs synthesis.

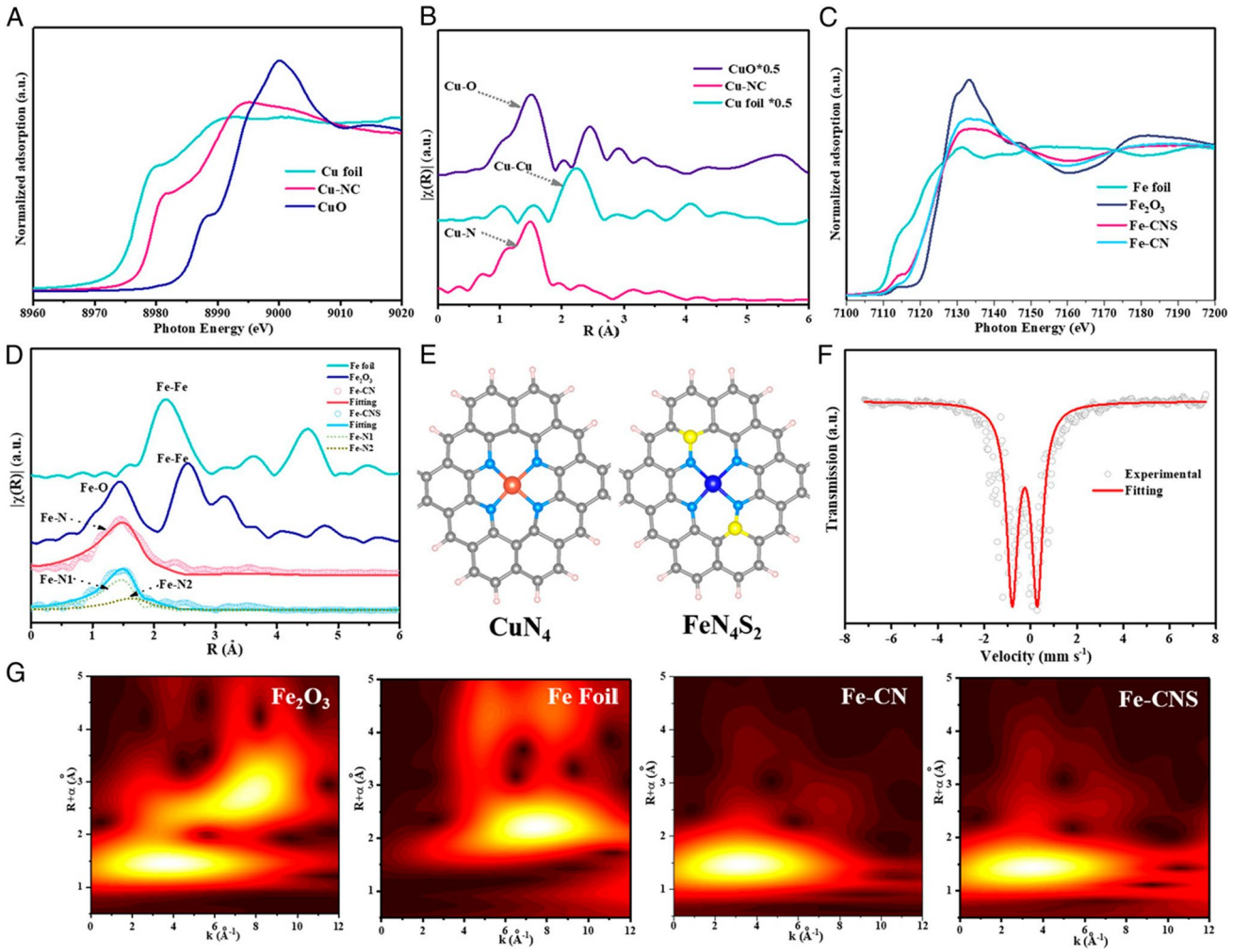

Fig. 4 **a** XANES spectra of Cu-CN, Cu foil and CuO at the Cu K-edge and **b** the corresponding k^2-weighted EXAFS spectra; **c** XANES spectra of Fe-CN, Fe-CNS, Fe foil, and Fe_2O_3 at the Fe K-edge and **d** the corresponding k^2-weighted EXAFS spectra; **e** fitted configurations of CuN_4 and FeN_4S_2 in Cu-CN and Fe-CNS; **f** ^{57}Fe Mössbauer spectra of Fe-CN SACs; **g** WT-EXAFS analysis of Fe_2O_3, Fe Foil, Fe-CN, and Fe-CNS. (Reprinted with permission from Ref. [35]. Copyright 2021 the National Academy of Sciences)

Zhang et al. synthesized 2D MOF materials with nut-like morphology and pyrolyzed them into carbon-based Fe SACs [37]. Based on HAADF-STEM, XPS, XAS, etc., the isolated Fe SACs with FeN_2O_2 coordination structure have been identified. Excellent FE of about 92% at − 0.68 V and NH_3 production rate of ~ 46 mg/h/mg_{cat} (about 9.2 mg/h/cm^2) at − 0.88 V have been achieved in neutral electrolytes. The mechanistic studies using in-situ Ramen and DFT calculations suggested that the N,O-doping would tune the Fe d-band and alter the adsorption energy of intermediates. The FeN_2O_2 showed better conductivity and NH_3 selectivity than the FeN_4 coordination. In addition, the FeN_2O_2 configuration could promote the conversion of HNO^* to N^* and thus the selective and efficient production of NH_3. Liu et al. fabricated Fe SACs with different coordination structures by thermal modulation (see Fig. 5). The feedstocks of $FeCl_3$, alanine and melamine were thoroughly mixed and ball milled, which then underwent a two-stage pyrolysis and carbonization treatment under inert atmosphere [38]. Combined with various characterizations, the Fe coordination environments were resolved as OH-Fe-N_4, Fe-N_3, and Fe-N_4 respectively for the materials pyrolyzing at 800, 900 and 1000 °C. The unique Fe-N_3 configuration exhibited the best catalytic performance, which realized the optimal FE of ~ 86% at − 0.7 V and the highest NH_3 yield rate of 18.8 mg/h/mg_{cat}. at − 0.9 V. The mechanisms have been investigated by the *operando* ATR-SEIRAS and DFT calculations. The work addressed the influences of different Fe coordination patterns with N and O on NO_3RR to NH_3.

The engineering of carbon materials as the support could also considerably affect the catalytic performance. Wang et al. utilized the harmful algae biomass as the feedstock to synthesize the carbon-supported Fe SACs to catalyze the NO_3RR [39]. The catalyst materials were simply obtained by pyrolyzing algae and Fe precursor with KOH activation at 800 °C. A variety of characterizations have been conducted to confirm the atomically-dispersed structure and the electronic states. Under optimal conditions, the highest NH_3 production rate was ~ 20 mg/h/mg_{cat} (~ 165 mg/h/cm^2) and the FE was 87.3%. The catalyst maintained good stability after continuous operation of beyond 50 h. Based on the experimental and DFT calculation results (see Fig. 6), the Fe-N_4 site has diminished the energy barriers and enhanced NO_3RR performance. Besides, the downstream coupling of NH_3 with CO_2 to produce urea has been demonstrated and the carbon footprint mitigation potentials of the proposed method has been analyzed. This study utilized waste biomass resources for material synthesis which created extra values on sustainability and environmental protection.

Song et al. prepared Fe SACs on g-C_3N_4 support by one-step pyrolysis method [40], which demonstrated an excellent nitrogen removal ability of 9857.5 mg N/g_{Fe} and a high FE of 77.3% at − 0.65 V. The catalyst could effectively promote NO_3RR at a low NO_3^- concentration of 50 mg/L, which offers an idea on support design for low concentration nitrate reduction to facilitate the practical application to use wastewater as the feedstock. Ren et al. reported the synthesis of Fe SACs on MXene nanosheets as a nanohybrid filter by vacuum filtration onto PTFE membrane, and the NO_3RR was conducted in a flow-through configuration in neutral conditions [41]. The single atom nature of Fe (1.7 wt% loading) was verified by different characterizations. The highest nitrogen removal rate was 97.2% with the NH_3 selectivity of 99.2%, and the highest FE of ~ 83%. The FE could keep beyond 80% after 10 h continuous operation. The DFT calculations suggest that the Fe SACs on MXene notably inhibited the HER side reaction and mitigated the energy barrier of the limiting step of converting NO* to HNO* compared to the Fe NPs on MXene (see Fig. 7). Very recently, Genoux et al. have first reported a new crystalline carbon nitride material with a general formula of $C_6N_9H_2Fe_{0.4}Li_{1.2}Cl$ (abbreviated as PTI/$FeCl_2$), in which the Fe sites were all with the same chemical environment [42]. The material was obtained by reacting PTI/LiCl with a low-melting $FeCl_2$/KCl flux and then anaerobic rinsing with methanol. The Fe (in the oxidation state of + 2) was

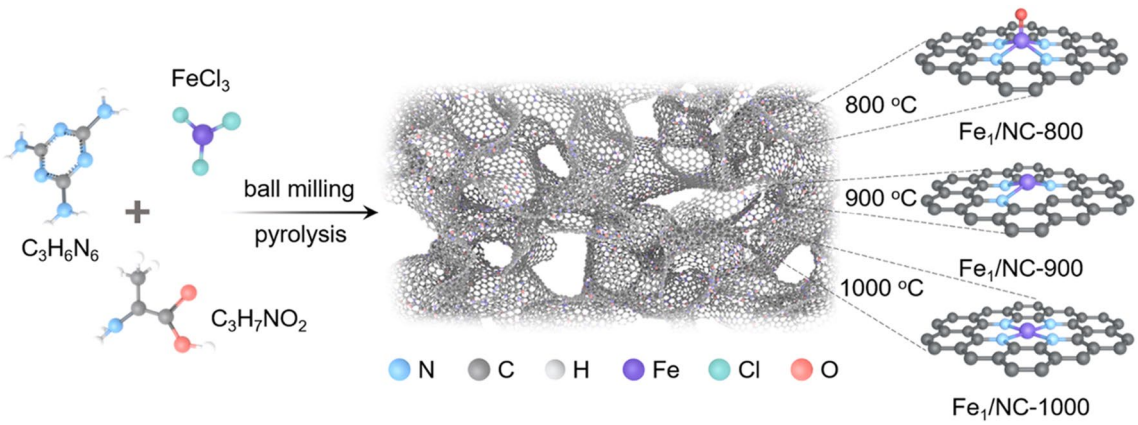

Fig. 5 Schematic of the synthesis process for Fe_1/NC-X (Reprinted with permission from Ref. [37]. Copyright 2023 the Elsevier)

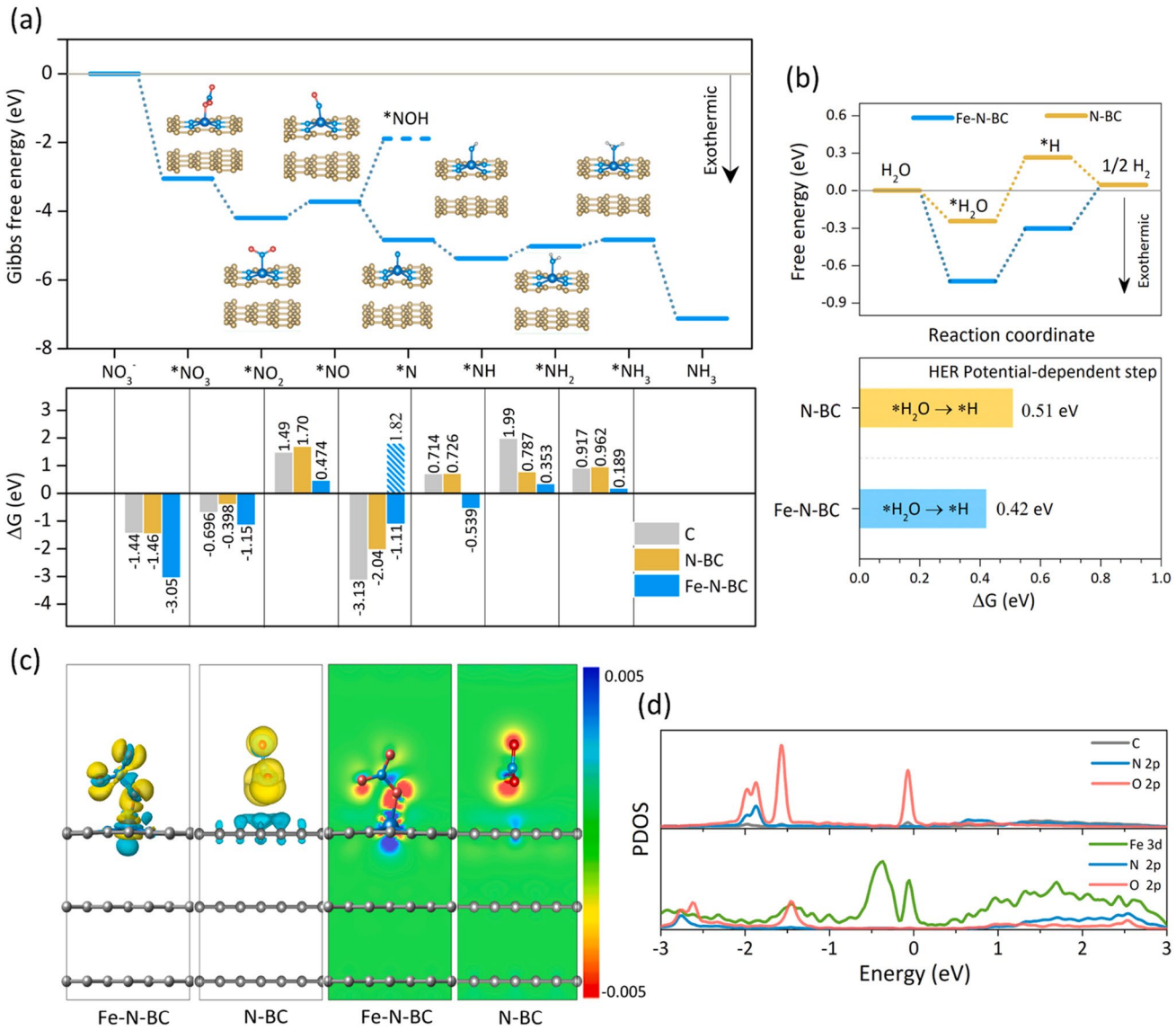

Fig. 6 The DFT calculation results of Fe-N-BC. **a** Gibbs free energy diagram of NO_3RR occurring on Fe-N-BC surface (upper) and the change in Gibbs free energy between the steps on different surfaces (lower); **b** the reaction energies of H_2 formation and PDS energy barriers over N-BC and Fe-N-BC; **c** differential charge density plot of NO_3^- adsorbed on the surface; **d** PDOS of Fe-N-BC and N-BC with NO_3^- adsorbed (Reprinted with permission from Ref. [39]. Copyright 2023 the Elsevier)

atomically dispersed with $FeCl_2N_2$ coordination environment. The material could promote NO_3RR with NH_3 production rate of 0.1 mmol/h/cm^2 and a FE of ~ 80% at − 0.8 V. The above works show the considerable effect of carbon species as support for Fe SACs and the rational selection or preparation of the carbon materials is important.

Fabricating dual-atom catalysts by coordinating the Fe with a second atomically-dispersed metal species would add on new possibilities on structure engineering and overcome the limited linear scaling relations of one specific site to promote multi-electron transfer. The Fe-Cu dual-metal catalysts have been reported by Zhang et al. [43]. To form well-dispersed metal–metal dimer sites, the carbon support (denoted as holey nitrogen-doped graphene, HNG) was obtained from GO through nitric acid oxidation, urea hydrothermal and annealing treatments (see Fig. 8). Then, the Fe and Cu precursors were added with the carbon support for pyrolysis treatment to obtain the Fe-Cu/HNG. The HAADF-STEM images have clearly revealed the diatomic pair structure of the as-synthesized catalysts with a distance of ~ 2.3 Å which was similar with the bond length of Fe-Cu by simulation. The EDX and EELS confirmed the coexistence of the Fe and Cu elements. The carbon support was relatively mesoporous with a high surface area of 858 m^2/g, and only the peaks assigned to the carbon support were observed on XRD. The XPS analysis unraveled the potential electron transfer from

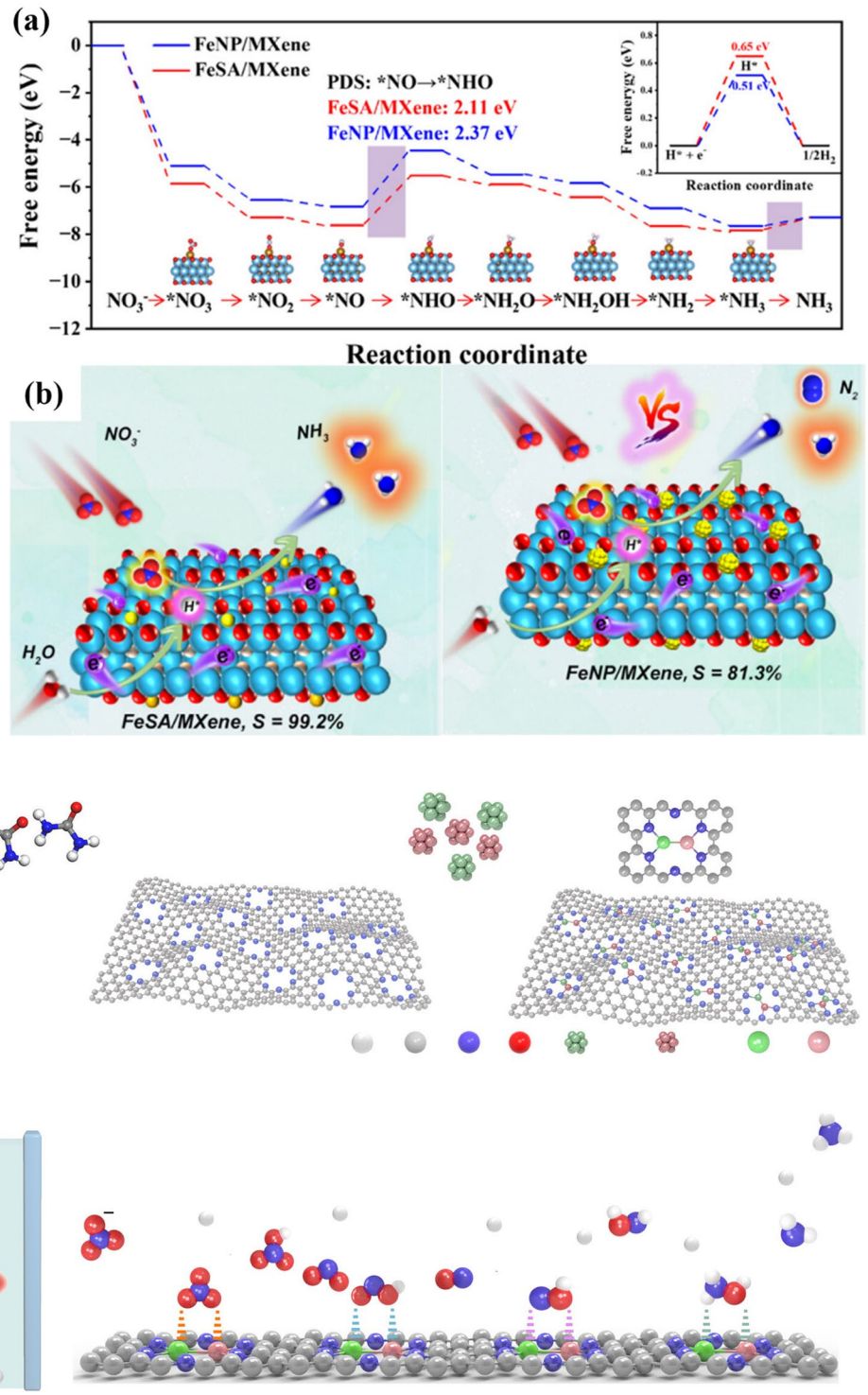

Fig. 7 **a** Gibbs free energy diagrams of nitrate reduction to NH_3 and H_2 evolution reaction (the top right) over FeSA/MXene and FeNP/MXene; **b** proposed mechanism for electrocatalytic reduction of nitrate on the FeSA/MXene and FeNP/MXene filters (Reprinted with permission from Ref. [41]. Copyright 2023 the American Chemical Society)

Fig. 8 Schematic illustration of the synthesis of Fe-Cu/HNG and the electrochemical reduction (Reprinted with permission from Ref. [43]. Copyright 2023 the Springer Nature)

Fe to Cu in the dual-atom catalysts. Based on the XAF results, the dominant Fe-N or Cu-N sites and the minor portion of Fe-Cu sites were identified. The Cu and Fe atoms were in oxidized states and electron transfer from Fe to Cu was substantiated which was in agreement with XPS. The Fe-Cu/HNG catalysts could promote NO_3RR at relatively low overpotentials, with a high FE of 92.5% at − 0.3 V and NH_3 production rate of 1.1 mmol/h/mg at − 0.5 V. The DFT calculations implies that

the Fe-Cu sites could intensely interact with the NO_3^- to boost the adsorption and discharge, and also weaken the N–O bonds to decrease the overall reaction barriers.

Apart from the above works, computational studies on the catalyst design and selection for NO_3RR have also been reported. Huang et al. employed DFT calculations to screen Fe-based MOFs with the salophen unit [44], and the computational analysis pointed out that the FeN_2O_2 with the inherent semi-enclosed structure would be more catalytically active than the commonly-reported FeN_4 coordination structure. The FeN_2O_2 geometry boasted smaller energy gap between unoccupied d_z^2 and occupied d_{yz} electron states to boost the adsorption and activation of the key NO* intermediate. Shu et al. utilized the spin-polarized first-principle calculations to investigate the synergistic effects of dual-metal sites for NO_3RR which could guide future studies on catalyst development for the reaction [45]. More than 20 dual-atom candidates have been scrutinized, of which the FeMo/g-CN and CrMo/g-CN displayed the best performances with lower overpotentials (− 0.34 V and − 0.39 V respectively). The dual-metal synergy could be ascribed to the coupling of the metal dimer *d* orbitals with the antibonding orbital of NO_3^-. In addition, the dual-metal sites on the support have considerably declined the bandgap of the support for potential photocatalytic conversion.

4 Conclusions and future remarks

The NO_3RR furnishes a "one-stone, two-birds" solution for wastewater treatment and green NH_3 production to fight against global warming. As an emerging field, constant and intensive efforts are anticipated to push the advances of the technology towards future industrialization. For the practical uses of the NO_3RR, the selection of the catalyst material is unambiguously principal. Compared to the noble metal catalysts and the Fe NPs, the carbon-based Fe SACs boast exceptional merits in regards of the price, selectivity, durability and efficiency. Due to the unique quantum confinement effect and the high valence of Fe SACs, the surface free energy of the Fe atoms has been maximized to promote the adsorption and activation of the substrate with maximal atom efficiency. The strong SMSI could enable high durability of the Fe SACs. Because of these special advantages, carbon-based Fe SACs are one of the most promising candidate catasysts for NO_3RR to NH_3. The rational design of Fe SACs including the carbon support design, the coordination environment adjustment (different geometry), the preparation parameter optimizations and so on are of vital importance for improved catalytic performances.

The major challenges in Fe SACs preparation are normally that the FE and NH_3 production rate were not quite high currently which required further catalyst engineering to improve. Besides, the durability needs to be enhanced to eventually be suitable for industrial uses. To boost the FE and NH_3 production rate, future directions could be the preparation of high loading Fe SACs on carbon support. The loading amount was usually low to obtain atomically dispersed Fe SACs but it will reduce the amounts of overall active sites. The development of high loading Fe SACs could offer more surface active sites to promote the reaction within a short period of time and high production rate. Besides, the construction of hierarchical porous carbon supports is favorable to improve the mass and electron transfer to enable fast kinetics for NO_3RR. To achieve good stability, the SMSI effect should be elaborately utilized to prevent the aggregation or leaching of the Fe SAC species. The different influences of coordination species (N, O, P, S, etc.) and geometry (FeN_3, FeN_4, FeN_2O_2, etc.) are required to be investigated in detail with more systematic characterizations to elucidate the structure-activity relationships and identify the key structural factors.

In terms of sustainability, the preparation process of the carbon-supported Fe SACs could be further modified. One future direction could be the utilization of waste biomass feedstocks for the preparation of carbon support materials. There are various technologies available to obtain porous carbon materials from biomass such as cellulose, woody waste, oceanic waste, etc. Waste biomass-derived carbon materials are satisfactory candidates to fabricate Fe SACs which may mitigate the capital costs and the carbon footprints. The advanced technologies for carbon material production from biomass could be systematically studied to unveil the key structure parameters of the carbon support to affect the catalytic performance. Meanwhile, the demonstrations of NO_3RR coupling with green electricity should be achieved to justify the low carbon emission of the process. Apart from electrochemical reduction, new catalytic materials may be devised and fabricated to perform photoelectrochemical or photocatalytic reduction of nitrate to produce NH_3. The incorporation of these technologies could directly utilize solar energy to prompt the reaction with a more satisfactory mitigation on carbon emission. Lastly, to realize wastewater treatment and NH_3 production at the same time, the catalytic systems should be versatile and robust to get rid of the influences of the complex contaminants in wastewater streams, as well as to effectively reduce the nitrate pollutant at a relatively low concentration.

Acknowledgements This work was financially supported by the Shenzhen Science and Technology Innovation Committee (KCXFZ20201221173413038).

Author contributions XC drafted the manuscript, XJ edited the manuscript and drew Figs. 1 and 2, and JK collected the references and prepared Table 1. All authors reviewed the manuscript.

Declarations

Competing interests The authors declare no competing interests.

References

1. Chehade G, Dincer I. Progress in green ammonia production as potential carbon-free fuel. Fuel. 2021;299:120845.
2. Olabi A, Abdelkareem MA, Al-Murisi M, et al. Recent progress in green ammonia: production, applications, assessment; barriers, and its role in achieving the sustainable development goals. Energy Convers Manag. 2023;277:116594.
3. MacFarlane DR, Cherepanov PV, Choi J, et al. A roadmap to the ammonia economy. Joule. 2020;4:1186–205.
4. Yan N, Chen X. Sustainability don't waste seafood waste. Nature. 2015;524:155–7.
5. Xie S, Jia C, Go Ong SS, et al. A shortcut route to close nitrogen cycle: bio-based amines production via selective deoxygenation of chitin monomers over Ru/C in acidic solutions. iScience. 2020;23:101096.
6. Dai J, Li F, Fu X. Towards shell biorefinery: advances in chemical-catalytic conversion of chitin biomass to organonitrogen chemicals. ChemSusChem. 2020;13:6498–508.
7. Chen X, Yan N. Conversion of chitin to nitrogen-containing chemicals. Chem Catal Biomass Upgrad. 2020;28:569–90.
8. Chen X, Song S, Li H, et al. Expanding the boundary of biorefinery: organonitrogen chemicals from biomass. Acc Chem Res. 2021;54:1711–22.
9. Sagawa T, Kobayashi H, Fukuoka A. Effect of Lewis acid on catalytic dehydration of a chitin-derived sugar alcohol. Mol Catal. 2020;498:111282.
10. Ma X, Gözaydın G, Yang H, et al. Upcycling chitin-containing waste into organonitrogen chemicals via an integrated process. Proc Natl Acad Sci USA. 2020;117:7719–28.
11. Zheng Y, Xu D, Zhang L, et al. Base-free air oxidation of chitin-derived glucosamine to glucosaminic acid by zinc oxide-supported gold nanoparticles. Chem Asian J. 2022;17:e202200556.
12. Techikawara K, Kobayashi H, Fukuoka A. Conversion of *N*-acetylglucosamine to protected amino acid over Ru/C catalyst. ACS Sustain Chem Eng. 2018;6:12411–8.
13. Wang Y, Kou J, Wang X, et al. Acid hydrolysis of chitin in calcium chloride solutions. Green Chem. 2023;25:2596–607.
14. Kobayashi H, Suzuki Y, Sagawa T, et al. Selective synthesis of oligosaccharides by mechanochemical hydrolysis of chitin over a carbon-based catalyst. Angew Chem Int Ed. 2023;62:e202214229.
15. Gözaydın G, Sun Q, Oh M, et al. Chitin hydrolysis using zeolites in lithium bromide molten salt hydrate. ACS Sustain Chem Eng. 2023;11:2511–9.
16. Zhang A, Wang C, Chen J, et al. Efficient enzymatic hydrolysis of chitin into *N*-acetyl glucosamine using alkali as a recyclable pretreatment reagent. Green Chem. 2021;23:3081–9.
17. Bobbink FD, Zhang J, Pierson Y, et al. Conversion of chitin derived *N*-acetyl-D-glucosamine (NAG) into polyols over transition metal catalysts and hydrogen in water. Green Chem. 2015;17:1024–31.
18. Ji X, Kou J, Gözaydın G, et al. Boosting 3-acetamido-5-acetylfuran production from *N*-acetyl-D-glucosamine in γ-valerolactone by a dissolution-dehydration effect. Appl Catal B-Environ. 2023;342:123379.
19. Chen K, Wu C, Wang C, et al. Chemo-enzymatic protocol converts chitin into a nitrogen-containing furan derivative, 3-acetamido-5-acetylfuran. Mol Catal. 2021;516:112001.
20. Shi X, Ye X, Zhong H, et al. Sustainable nitrogen-containing chemicals and materials from natural marine resources chitin and microalgae. Mol Catal. 2021;505:111517.
21. Qiu W, Liu Y, Xie M, et al. Structural engineering of catalysts for ammonia electrosynthesis from nitrate: recent advances and challenges. EES Catal. 2024. https://doi.org/10.1039/D3EY00184A.
22. Wang C, Zhang Y, Luo H, et al. Iron-based nanocatalysts for electrochemical nitrate reduction. Small Methods. 2022;6:2200790.
23. Liu Y, Liu K, Wang P, et al. Electrocatalytic upcycling of nitrogenous wastes into green ammonia: advances and perspectives on materials innovation. Carbon Neutrality. 2023;2:14.
24. Liu D, Qiao L, Peng S, et al. Recent advances in electrocatalysts for efficient nitrate reduction to ammonia. Adv Funct Mater. 2023;33:2303480.

25. Cerrón-Calle GA, Wines A, Garcia-Segura S. Atomic hydrogen provision by cobalt sites in a bimetallic Ni/Co(OH)$_x$ and trimetallic Ni/Cu$_2$O/Co(OH)$_x$ configurations for superior ammonia production. Appl Catal B-Environ. 2023;328:122540.
26. van Langevelde PH, Katsounaros I, Koper MT. Electrocatalytic nitrate reduction for sustainable ammonia production. Joule. 2021;5:290–4.
27. Garcia-Segura S, Lanzarini-Lopes M, Hristovski K, et al. Electrocatalytic reduction of nitrate: fundamentals to full-scale water treatment applications. Appl Catal B-Environ. 2018;236:546–68.
28. Yuan C, Lu Z, Jiang W, et al. Promoted NN activation by oxygen and boosted ammonia production over $Bi_4O_5Br_2$. Mol Catal. 2021;515:111913.
29. Qiao B, Wang A, Yang X, et al. Single-atom catalysis of CO oxidation using Pt_1/FeOx. Nat Chem. 2011;3:634–41.
30. Wang X, Zhang B, Chen X. Selective hydrogenation of lignocellulosic biomass over single-atom catalysts. Sustain Energy Fuels. 2023;7:2974–90.
31. Wang A, Li J, Zhang T. Heterogeneous single-atom catalysis. Nat Rev Chem. 2018;2:65–81.
32. Yang X-F, Wang A, Qiao B, et al. Single-atom catalysts: a new frontier in heterogeneous catalysis. Acc Chem Res. 2013;46:1740–8.
33. Wu Z-Y, Karamad M, Yong X, et al. Electrochemical ammonia synthesis via nitrate reduction on Fe single atom catalyst. Nat Commun. 2021;12:2870.
34. Li P, Jin Z, Fang Z, et al. A single-site iron catalyst with preoccupied active centers that achieves selective ammonia electrosynthesis from nitrate. Energy Environ Sci. 2021;14:3522–31.
35. Li J, Li M, An N, et al. Atomically dispersed Fe atoms anchored on S and N-codoped carbon for efficient electrochemical denitrification. Proc Natl Acad Sci USA. 2021;118:e2105628118.
36. Xu J, Zhang S, Liu H, et al. Breaking local charge symmetry of iron single atoms for efficient electrocatalytic nitrate reduction to ammonia. Angew Chem Int Ed. 2023;62:e202308044.
37. Zhang W-D, Dong H, Zhou L, et al. Fe single-atom catalysts with pre-organized coordination structure for efficient electrochemical nitrate reduction to ammonia. Appl Catal B-Environ. 2022;317:121750.
38. Liu L, Xiao T, Fu H, et al. Construction and identification of highly active single-atom Fe_1-NC catalytic site for electrocatalytic nitrate reduction. Appl Catal B-Environ. 2023;323:122181.
39. Wang H, Man S, Wang H, et al. Grave-to-cradle upcycling of harmful algal biomass into atomically dispersed iron catalyst for efficient ammonia electrosynthesis from nitrate. Appl Catal B-Environ. 2023;332:122778.
40. Song Q, Li M, Hou X, et al. Anchored Fe atoms for NO bond activation to boost electrocatalytic nitrate reduction at low concentrations. Appl Catal B-Environ. 2022;317:121721.
41. Ren Y, Tian F, Jin L, et al. Fluidic MXene electrode functionalized with iron single atoms for selective electrocatalytic nitrate transformation to ammonia. Environ Sci Technol. 2023;57:10458–66.
42. Genoux A, Pauly M, Rooney CL, et al. Well-defined Iron sites in crystalline carbon nitride. J Am Chem Soc. 2023;145:20739–44.
43. Zhang S, Wu J, Zheng M, et al. Fe/Cu diatomic catalysts for electrochemical nitrate reduction to ammonia. Nat Commun. 2023;14:3634.
44. Huang Y, Tang C, Li Q, et al. Theoretically developing the iron salophen-based organic framework for electrocatalytic nitrate reduction and revealing the origin of higher activity versus Fe-N_4-C. Mol Catal. 2023;549:113456.
45. Shu Z, Chen H, Liu X, et al. High-throughput screening of heterogeneous transition metal dual-atom catalysts by synergistic effect for nitrate reduction to ammonia. Adv Funct Mater. 2023;33:2301493.